Performance analysis of a nitrogen-based Brayton cryocooler prototype

Energy 290 (2024) 130095

Contents lists available at ScienceDirect

Energy

journal homepage: www.elsevier.com/locate/energy

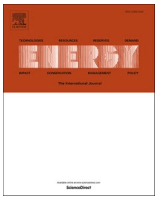

Performance analysis of a nitrogen-based Brayton cryocooler prototype

Alessandro Biglia [a,1], Matteo Bilardo [b,1], Lorenzo Comba [a], Davide Ricauda Aimonino [a], Marco Grella [a], Enrico Fabrizio [b,*], Paolo Gay [a]

[a] Department of Agricultural, Forest and Food Sciences (DiSAFA) – Università degli Studi di Torino, Largo Paolo Braccini 2, 10095, Grugliasco, TO, Italy
[b] TEBE Research Group, Department of Energy (DENERG) – Politecnico di Torino, Corso Duca Degli Abruzzi 24, 10129, Torino, TO, Italy

ARTICLE INFO

Handling Editor: L Luo

Keywords:
Brayton cycle
Innovative configuration
Thermodynamic performances
Thermal heat recovery
Eco-friendly gas

ABSTRACT

When very low temperatures are needed for industrial applications, reverse Brayton cryocoolers can be adopted. This paper reports the results of an energy analysis in which the performance of a Brayton cryocooler prototype was studied. The prototype is innovative in both the cycle configuration and the pressure and temperature levels. Moreover, nitrogen, an eco-friendly gas that is safe for people, was used as the working fluid.

Simultaneous measurements of the pressure and temperature at the inlet and outlet of the main thermodynamic cycle components, nitrogen flow rate, and power consumption were taken during the experimental tests. The prototype was tested at design operating conditions (maximum and minimum pressure of 18.5 and 8 bar respectively, and minimum temperature of −120 °C), obtaining a cooling effect of 15.6 kW, a temperature reduction rate at the turbine outlet of 8 °C min^{-1}, and a coefficient of performance of 0.29, which rises to 1.34 when including the waste heat (about 55 kW) that can be recovered at low temperatures (<100 °C). Also, a sensitivity analysis was carried out by testing the prototype at different maximum pressure and minimum temperature levels. The higher the maximum pressure, the higher the prototype performance is, and a minimum temperature of about −140 °C was reached. Our findings demonstrated that the tested prototype shows great promise for several industrial applications where low temperatures are required.

1. Introduction

The need for low temperatures for cooling and/or freezing purposes has allowed the growth and diffusion of cryogenic applications. Research in the cryogenic field has led to the development of two main categories of cryocoolers which are based on recuperative cycles or regenerative cycles.

In a recuperative cycle, the working fluid flows between two fixed pressure levels maintained by a compressor. All recuperative cycles share a separate flow heat exchanger to recover part of the heat between the flows at different pressures. Typical recuperative cycles include the Joule-Thomson (JT), Brayton, and Claude cycles. They differ in the expansion process, for example in a JT cycle the working fluid expands through a valve (JT valve) or a capillary tube, while in a Brayton cycle, the expansion occurs in a turbine. The Claude cycle combines the previous ones, and the expansion phases are often divided with recuperators. On the contrary, regenerative cycles are characterised by an oscillatory flow. The pressure levels are not fixed but vary according to appropriate phase angles between the cold and hot ends. The main equipment that makes up the regenerative cycles are a compressor and a displacer piston, separated by an evaporator, a regenerator, and a condenser. The maximum cooling effect is obtained when the same phase is reached between the flow and the pressure at the cold end. The working fluid is moved by the displacer piston between the cold and hot ends of the regenerator, which recovers the expansion work. Among the most popular regenerative cycles are the Stirling and the Gifford-McMahon (GM) cycles. The difference between them lies in the main compression method, which takes place using a valveless compressor (pressure oscillator) in the Stirling cycle, while a less expensive conventional compressor with inlet and outlet valves (or a scroll compressor) is used in the GM cycle. An alternative to the most common regenerative cycles is the pulse tube cycle, in which the displacer piston is replaced by a pulse tube. This solution, by eliminating the displacer moving parts, considerably reduces vibrations, making it useful for various applications. The tube is kept adiabatic, and the working fluid temperature varies according to the primary source of pressure oscillation (Stirling or GM). Table 1 highlights the pros and cons of some

* Corresponding author.
E-mail addresses: alessandro.biglia@unito.it (A. Biglia), matteo.bilardo@polito.it (M. Bilardo), enrico.fabrizio@unito.it (E. Fabrizio).
[1] Co-first authors.

https://doi.org/10.1016/j.energy.2023.130095
Received 24 July 2023; Received in revised form 15 December 2023; Accepted 20 December 2023
Available online 13 January 2024

Nomenclature

EH	Electric heater
EM	Electric motor
HX1	Heat exchanger (aftercooler)
HX2	Heat exchanger (intercooler)
HR	Heat exchanger (recuperator)
K1	Reciprocating compressor
K2	Centrifugal compressor
P_{eh}	Electric heater power [kW]
P_{hx1}	Released heat in the HX1 heat exchanger [kW]
P_{hx2}	Released heat in the HX2 heat exchanger [kW]
T1	Turbine
V1 – V4	Regulation valves
X_i	Measured parameters
ΔX_i	Uncertainty of the measured parameters
ΔY	Uncertainty of the derived parameters

cryocooler examples.

1.1. State of the art in cryocoolers applications

Research has made it possible to achieve promising results both in terms of the feasibility and reliability of cryocoolers. Table 2 reports examples of cryocooler applications developed in recent years. Among the sectors most affected by the diffusion of cryocoolers are certainly those of space applications and superconductors, which operate at temperatures lower than 80 K by usually adopting helium as the working fluid. In 2011, Choi et al. [6] studied the cool-down characteristics of a 3 T superconducting magnet using a helium cryocooler in a two-stage GM cycle, reaching 1 W at 4.5 K. Other recent applications concern the studies by Qiao et al. (2021) [7], which developed a helium Stirling cryocooler for superconductors cooling capable of providing 1048 W at 77 K with a relative Carnot efficiency equal to 26.1 %. The same system, optimised by the authors, was able to reach 130.2 W at 20 K without thermal load, with a relative Carnot efficiency equal to 27.2 %. In the field of space cryogenics, applications require very low temperatures,

Table 1
Comparison between recuperative and regenerative cycles.

Type	Cycle	Working fluid	Temperature range [K]	Pressure Range [bar]	Advantages	Disadvantages	Ref.
Recuperative	Joule - Thomson	Nitrogen Nitrogen/Hydrocarbon	30–80	150–200	Small size Low mass Low vibration	Low cooling capacity Low compression Efficiency	[1]
	Brayton	Neon, Helium	65–280	1–3	High reliability High thermodynamic efficiency Expansion work recovery	High production costs High mass and size	[2]
	Claude	Neon, Helium, Nitrogen/ Hydrocarbon	6–70	1–3	Low compression ratio Expansion work recovery	High production costs High mass and size High vibration	[2]
Regenerative	Stirling	Helium	20–300	10–35	Reduced size and mass Easy maintenance High efficiency	Low lifetime Low cooling capacity High vibration	[3]
	Gifford-McMahon	Helium	3–150	5–30	Low production cost High reliability	High maintenance costs	[4]
	Pulse tube	Helium	3–200	10–30	No moving parts Low power consumption Low vibration	Low cooling capacity High cost of tubes Performance depends on the tube length	[5]

Table 2
Examples of cryocoolers applications.

Application	Fluids	Cycle	Temperature [K]	Cooling capacity [W]	Relative Carnot efficiency [%]	Ref.
Superconductors	Helium	Two Stage GM	4.5–50	1–27	–	[6]
	Helium	Stirling	77	1048	26.1	[7]
	Helium	Stirling	20–77	130.2–274.8	27.2	[8]
Space	Superfluid Helium	–	1.3–2	60–100		[9]
	Helium (^{4}He)	Brayton	20	20–80	23–26	[10]
	Helium (^{4}He) for Stirling Helium (^{3}He) for JT	Hybrid Stirling - JT	1–3	14.7–18.7 10^{-3}	–	[11,12]
	Helium (^{4}He)	Joule-Thomson	2.39	4 10^{-3}	–	[13]
Infrared detectors	Helium	Two Stage GM	80–122	290–390	5–9	[14]
	Neon	Pulse Tube	35–75.1	2–9	–	[15]
Electronic devices	Methane or Nitrogen	Joule-Thomson	101–138	8 - 131 10^{-3}	–	[16]
	Helium	Stirling	80	350	26.8	[17]
Gas liquefaction	Helium	Two Stage GM	4.2	1.5	–	[18]
	Nitrogen/Hydrocarbon	Joule-Thomson	90	10		[19]
	Nitrogen	Pulse Tube	52–110	46.6–129.2	21	[20]
Road transport	Air	Brayton	220–240	3.4–9.5 10^3	41 (real)	[21,22]
Food freezing	Air, Nitrogen	Brayton	120–150	3.5–16,10^3	6 - 30 (real)	[23,24]

thus reducing the cooling capacity. In Hirabayashi's work [8], the use of a superfluid helium tank made it possible to reach 60 W at 2 K for the AKARI satellite, with an expected lifetime of about one year. The need for longer space missions has introduced the use of mechanical cryogenic cycles. In 2014, Deserranno et al. [9], in collaboration with NASA, optimised a Brayton cryocooler to produce liquid hydrogen [10] in orbit, providing 20 W at 20 K with a relative Carnot efficiency of 23 %. In a recent work conducted in 2021, Zhang and Dang [11] tested a Stirling-JT hybrid cycle implementation capable of delivering 14.7 mW at 1 K for the next generation of space quantum information technology. Similarly, Liu et al. [12] have developed a compact cryocooler based on a hybrid cycle consisting of a four-stage JT cycle precooled by a two-stage pulse tube cycle. The results achieved in the laboratory demonstrated a cooling capacity of 4 mW at 2.4 K. A pulse tube cryocooler was also used for boil-off gas reliquefaction in liquid natural gas tanks [13].

Numerous cryogenic applications also regard industrial sectors at temperatures in the range of 30–180 K. Among these sectors, infrared detectors are certainly relevant. Interesting results were achieved by Jakob and Lizon [14], who developed a two-stage GM helium cryocooler designed for visible light transmittance instruments capable of providing cooling capacities between 290 and 390 W at temperatures of 80–122 K (5–9% relative Carnot efficiency). Recent developments in infrared energy management were instead achieved in 2021 by Guo et al. [15], where a cryogenic system based on a neon-powered pulse tube cryocooler was able to deliver from 2 to 9 W in a temperature range of 35–75 K. The general electronic devices sector is also becoming increasingly attractive for the development of ad-hoc cryocoolers. For example, a micromachined JT cryocooler was designed by Derking et al. [16] for small electronic devices needing a cooling effect in the range of 101–138 K (8–131 mW of cooling capacity). This system, with dimensions of 60 × 10 × 0.7 mm, uses nitrogen as a working fluid. An alternative solution for higher cooling capacities adaptable to electronic devices is the free-piston Stirling cryocooler developed by Zhu et al. [17], which is based on a helium cycle and capable of delivering 350 W at 80 K. The authors, thanks to a parametric optimisation of the developed prototype, reached a Carnot cycle efficiency of 26.8 %, also proposing the solution for the gas liquefaction sector. In fact, gas liquefaction is particularly widespread in the application of cryogenic cycles at industrial levels. The need for gas liquefaction is shared by numerous industrial sectors, starting from metal and steel ones, up to those of the food industry. Depending on the gas to be liquefied, different cryogenic cycles can be adopted. Using five two-stage GM cryocoolers with a capacity of 1.5 W at 4.2 K, Xu et al. [18] managed to optimise the production of liquid helium up to the liquefaction rate of 83 L per day. A system designed for the liquefaction of gases such as nitrogen, argon, oxygen or methane was developed by Dorosz et al. [19] using a single-stage JT cryocooler capable of delivering 10 W at 90 K. The authors developed a system made of mass-produced components to limit costs and encourage the reproducibility of the system on a large scale. Also, a pulse tube refrigerator for natural gas liquefaction was developed by Deng et al. [20]. The system, able to work in the temperature range of 52–110 K with a cooling capacity of 46.6–129.2 W, manages to reach a relative Carnot efficiency of 21 %, and compared to traditional liquefiers, its lightness and size certainly make it competitive in the gas liquefaction sector. Recuperative cycles based on the reverse Brayton plant configuration have also been studied and tested for road transport refrigeration systems [21,22]and food freezing [23,24].

Fig. 1 highlights the potential of the main cryocoolers analysed in terms of efficiency and temperature levels, highlighting the main fields of application. Fig. 1 also shows the families of refrigeration cycles that do not fall within cryocoolers, such as vapor compression, absorption cycles and Hampson-Linde cycles.

1.2. Advances and limits of Brayton and reverse-Brayton cycles in cryogenics applications

Among the various thermodynamic cycles harnessed for cryogenic purposes, the Brayton cycle and its reverse variant have emerged as noteworthy contenders. These cycles, traditionally associated with power generation and gas compression, have found a unique niche in the world of cryogenics, driven by their efficiency and adaptability. This section delves into the utilisation of Brayton and reverse-Brayton cycles in cryogenic systems, shedding light on their evolution and significance. To provide context, after having explored the broader landscape of thermodynamic cycles in cryogenic applications, the distinctive role played by Brayton cycles in achieving efficient and reliable cryogenic applications is now showcased.

In cryogenic applications, Brayton and reverse-Brayton cycles have demonstrated several advantages [25], both in closed and open cycles [26]. Notably, Chang and Cha [27] highlighted the flexibility and optimisation potential of reverse-Brayton cycles using gaseous helium

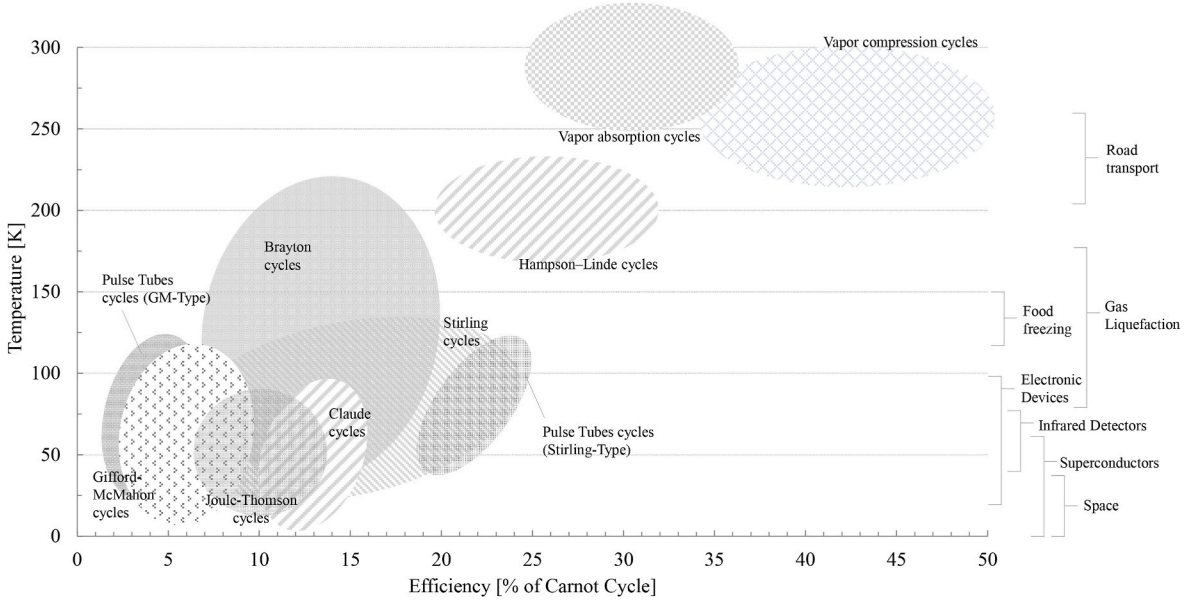

Fig. 1. Map of the main cryogenic and refrigeration cycles.

for cryogenic refrigeration, particularly in cooling superconducting magnets [28]. Bian et al. [29] discussed the efficiency gains and cost-effectiveness of Brayton cycles with LNG and helium in a novel hydrogen liquefaction process, emphasizing the importance of balancing efficiency, capital costs, and operational requirements. These cycles are known for their reliability and continuous operation, which are crucial in processes like cryogenic coolant production, ensuring consistent cooling [30]. Conklin et al. [31] underscored the safety and efficiency advantages of using nitrogen-based fluids in space power generation applications, given its non-flammable and lower mass-to-power ratio. Closed Brayton cycles have also proven critical for when it is necessary to maximize the compactness of cooling systems for power conversion units in space and underwater applications [32]. Moreover, Hou et al. [33] provided a comprehensive review of the advancements in reverse Brayton cycle cryocoolers, emphasizing the efficiency improvements achieved through advanced configurations, including the use of gas bearing in the turbo expander. These advantages, supported by scientific literature and engineering practices, make Brayton and reverse-Brayton cycles versatile and efficient choices for a range of cryogenic applications.

Along with the development of Brayton cycles, nitrogen has emerged as a valid working fluid in cryogenic applications due to its distinct advantages [34]. Notably abundant and cost-effective, nitrogen is readily available [35]. Its non-flammable and non-toxic nature enhances safety in confined cryogenic environments. With a wide operating temperature range spanning from its boiling point at −196 °C (−321 °F) to ambient temperature, nitrogen is versatile and suitable for both moderate and extremely low-temperature applications [36]. This versatility, combined with favourable thermodynamic properties that contribute to cycle efficiency, makes nitrogen an efficient choice [37]. Furthermore, its minimal environmental impact and compatibility with cryogenic materials underscore its role as an environmentally friendly and reliable working fluid in cryogenic systems [38].

A considerable example of coupling a Brayton cycle using nitrogen as the operating fluid is the study conducted by Olumayegun et al. [39], where the advantages of this solution were highlighted in terms of efficiency, safety, and plant size. Cao et al. [40] also relied on a novel nitrogen re-liquefaction cascade process based on a reverse-Brayton cycle, numerically studying different configurations of heat exchangers in the cryocooler. The authors obtained promising results in terms of reducing the mass-flow rate of the working fluid and lowering operating costs. The coupling of a Brayton cycle with nitrogen as the working fluid showed remarkable flexibility in the study by Chen et al. [41], who demonstrated how this type of plant solution was suitable for integration with other conventional cycles for the cascade recovery of LNG cryogenic energy, including renewable solar resources. Choi et al. [42] also highlighted the competitiveness that a nitrogen Brayton cycle could have in terms of cycle efficiency, compared to the conventional solutions of steam Rankine cycles. The authors numerically highlighted how a detailed turbine design led to a reduction in components size, without compromising cycle efficiency.

In conclusion, nitrogen-based Brayton and reverse-Brayton cycles have found diverse applications in cryogenics, ranging from superconducting magnet cooling to LNG production and space power generation. The studies highlighted in this review underscored the efficiency gains, safety advantages, and potential for optimisation in these applications. Nevertheless, challenges persist, such as operating temperature limitations and engineering complexities, which necessitate ongoing research to address these issues and unlock the full potential of nitrogen-based cryogenic cycles.

Although the use of Brayton cycles for cryogenic applications, combined with the exploitation of nitrogen as a working fluid, seems to be promising in many ways, there still remain some critical issues that need new research and more in-depth studies. In particular, the analysis conducted showed that:

- The solutions proposed in the literature for nitrogen Brayton cycles have a strong experimental gap. Most studies focus on numerical design proposals and optimisations, which are not supported by experimental evidence. The need for the prototyping of the numerically proposed solutions is therefore necessary for development in this area.
- Studies in the literature have little versatility and are often focused exclusively on niche applications with complex large-scale replicability. The deployment of nitrogen-based Brayton cycles needs broader proposals that can be adapted to different cryogenic industrial settings, improving the scalability of these cycles across multiple applications.
- The cryogenic powers tested for nitrogen Brayton cycles hardly exceed cooling capacities above a few hundred watts, reaching cryogenic temperatures under steady state conditions. These conditions further limit the deployment of such systems in industrial settings.

1.3. Aims of this work

This paper presents the results of an experimental campaign in which the performance of a nitrogen-based Brayton cryocooler prototype (Bc-prototype), suitable for several industrial applications at low temperatures, was tested. The Bc-prototype can operate at a maximum and minimum pressure of 18.5 and 8 bar respectively, and a minimum temperature of −120 °C (design conditions) by providing a cooling effect of 15.6 kW and about 55 kW of heat. A sensitivity analysis was also carried out by testing the prototype at different pressure and temperature levels. Nitrogen, which is an eco-friendly gas that is safe for people gas, was selected as the working fluid to comply with the guidelines of the European Commission (e.g. Green Deal).

The strength of the Bc-prototype lies in its configuration, which was designed to be suitable for different operating conditions and industrial scenarios (e.g. food industry), and on the combination of pressure and temperature levels, which guarantees high performance. An example of a possible application is indeed the one presented by the Authors in 2022 [24], where the Bc-prototype was used in a quick-freezing plant of fine meat at very low temperatures to increase the meat shelf life [43–45].

2. Materials and methods

To overcome the limitations of the Brayton cycles presented in the literature analysis (e.g., cooling effect range and versatility), an innovative Bc-prototype was designed and tested. The Bc-prototype involves new features regarding the scheme configuration, the temperature and pressure levels, and the adopted working fluid. Moreover, the Bc-prototype was designed to be adopted by several industrial applications. A feasibility study was conducted by the Authors [46], and a cycle modelling framework developed to identify efficient operative settings and to assess, via sensitivity analysis, how energy performance is affected by the temperature and pressure levels. The design temperature at the Bc-prototype turbine outlet was set to −120 °C as a requirement of a project in which the final aim was to freeze different kinds of food products at very low temperatures [24]. The pressure level was selected according to the feasibility study and data of the Bc-prototype components (no turbomachineries were ad-hoc designed in order to limit the costs). No brands of the Bc-prototype components can be reported in the manuscript.

2.1. Design of the Brayton cryocooler prototype

Nitrogen was used in the Bc-prototype cycle since it is a very safe, robust and eco-friendly working fluid [47]. Indeed, nitrogen does not have problems related to humidity or solidification at the design Bc-prototype operating temperatures. This simplifies the Bc-prototype layout as no specific equipment is required to remove humidity from the working fluid, thus also reducing operation and maintenance costs.

The Bc-prototype and its layout are reported in Fig. 2. The main Bc-

prototype components are one reciprocating compressor (K1), one electric motor (EM) connected to K1 and controlled by a variable speed drive, one turbine (T1) whose shaft drives a centrifugal compressor (K2), two heat exchangers where nitrogen rejects heat (HX1 and HX2), one electric heater (EH) to simulate the heat exchanger where nitrogen absorbs heat (cooling effect), and one heat exchanger used as a recuperator (HR) which allows the nitrogen to be precooled before expanding in the turbine, thereby reducing the turbine outlet temperature without increasing the expansion ratio. Cold water at about 14 °C, available where the Bc-prototype was assembled and tested, was used to cool HX1 and HX2. The adopted turbine - centrifugal compressor configuration is also known as the bootstrap unit.

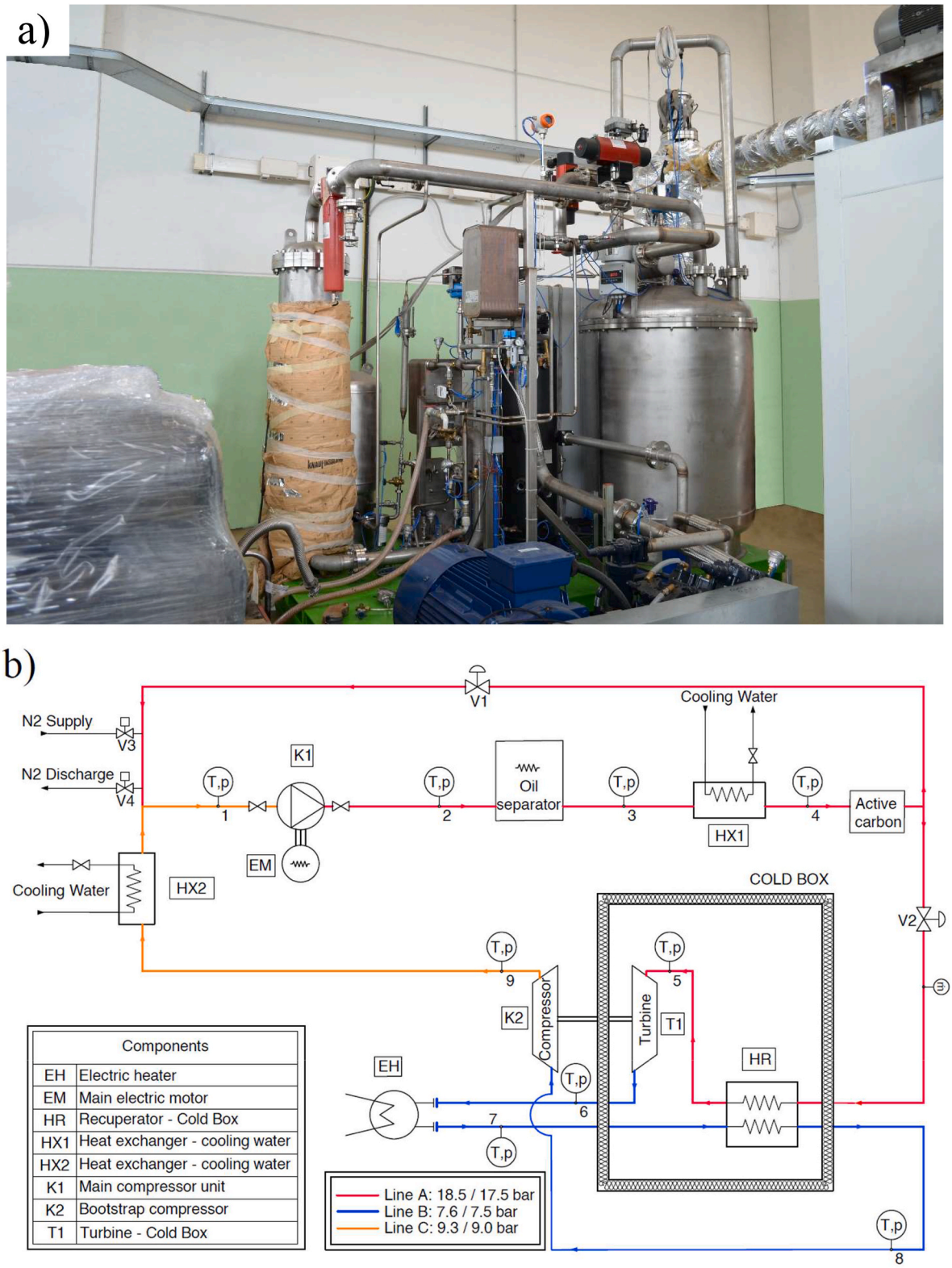

Fig. 2. The Brayton cryocooler prototype installed in the laboratory environment (a) with the functional design diagram of the main components and monitoring sensors (b).

When the electric motor starts driving the reciprocating compressor (K1), the V1 valve of the by-pass circuit (see Fig. 2b) opens and the V2 valve closes, while the V3 and V4 valves are used to regulate the nitrogen flow rate (supply and discharge) and thus the reciprocating compressor operating pressure. The electric motor and valves are automatically adjusted by the Bc-prototype control panel where the operating pressure is set. When the reciprocating compressor operates in steady-state conditions at its minimum speed, the V1 and V2 valves start closing and opening simultaneously and slowly.

At the V2 valve opening, some of the nitrogen flows into the turbine and undergoes an expansion stage, reducing its pressure and temperature. Also, the nitrogen expansion develops mechanical work to drive the centrifugal compressor (K2). The V2 valve opening must be properly controlled and adjusted to avoid turbine overspeed (a suitable value is between 65,000 and 70,000 rpm). According to the monitored speed and outlet temperature (cycle minimum value) of the turbine, the V2 valve is automatically controlled. The by-pass circuit is also used to avoid nitrogen flowing into the turbine in case of malfunctioning or during the Bc-prototype shutdown. Before the expansion phase in the turbine, the nitrogen undergoes cooling in the aftercooler (HX1), which is installed downstream of the reciprocating compressor (K1), and then in the recuperator (HR).

After the expansion phase and before entering the centrifugal compressor (K2), the nitrogen flows at low temperature in the electric heater (EH) where the cooling effect is simulated by providing heat, and then in the recuperator (HR) to absorb heat from the nitrogen entering the turbine. At the turbine start-up, the electric heater is kept off to reduce the time required to reach the desired turbine outlet temperature. When the electric heater is turned on to stabilise the cycle at the desired turbine outlet temperature, the reciprocating compressor is regulated to operate the Bc-prototype at steady-state conditions in terms of pressure and nitrogen flow rate too.

Since cooling a gas during compression is advantageous in terms of the work-input requirements, an intercooler (HX2) was installed between the two compressors to reduce the nitrogen temperature before entering the reciprocating compressor. The heat rejected by the nitrogen in the aftercooler (HX1) and intercooler (HX2) can be recovered to significantly increase the performance of the Bc-prototype.

Fourteen probes, connected to the electric panel, were used to measure the temperature (type T thermocouple – IEC 60584–1, ±0.5 K) and pressure (KELLER 23SX pressure transmitter, ±0.1 % of full scale) at the inlet and outlet of the Bc-prototype components as shown in Fig. 2b. Please notice that the nitrogen temperature measured at the reciprocating compressor outlet is affected by the lubricating oil temperature, which is used to cool the cylinders heads, which could not be measured. An oil filter was installed downstream of the reciprocating compressor to minimise the presence of oil in the turbine. The nitrogen mass flow rate was measured downstream the V2 valve (Flow sensor, CS INSTRUMENTS VA 550, ±1 % of measured value). The power input of the electric motor and of the electric heater were measured using a HOBO UX120 data logger (±0.1 % of full scale) connected to a split-core AC current sensor and to a WattNode 208/240 VAC 3 phase (±0.05 % of full scale). This means that when the V1 and V2 valves are opened simultaneously, only a fraction of the nitrogen mass flow rate is measured. However, the energy performance of the Bc-prototype is analysed only when the V1 and V2 valves are fully closed and opened respectively.

2.1.1. Design specifications and performance evaluation of the Bc-prototype

The main design data of the Bc-prototype presented in § 2.1 can be summarised as:

- A turbine outlet temperature of −120 °C. This value was selected for quick-freezing purposes in the food industry sector [23,24,43].
- A reciprocating compressor outlet pressure of 18.5 bar.
- A nitrogen flow rate of 0.52 kg s^{-1}.
- An electric heater power between 0 and 16 kW, which is used to simulate the cooling effect.
- A cycle Coefficient of Performance (COP) equal to 0.25 without considering the heat rejected in the aftercooler (HX1) and in the intercooler (HX2) that could be recovered.

The overall performance of the thermodynamic cycle deployed by the Bc-prototype was summarised through the performance indicators of COP and TER. The COP parameter only considers the cooling effect over the total electrical energy expenditure, while the parameter named TER (Total Efficiency Ratio) considers the sum of the useful effects (cooling and heating) over the entire system and the total electrical energy expenditure calculated over a defined period. The COP and TER parameters are calculated using Eqs. (1) and (2) as follows

$$COP = \frac{\int_0^T P_{eh}\,dt}{\int_0^T P_{em}\,dt} \tag{1}$$

and

$$TER = \frac{\int_0^T P_{eh}\,dt + \int_0^T P_{hx1}\,dt + \int_0^T P_{hx2}\,dt}{\int_0^T P_{em}\,dt} \tag{2}$$

where P_{eh} is the electric heater power [kW], that is the cooling effect, over the considered time period T (yellow lines in Figs. 3–8), P_{hx1} and P_{hx2} is the released heat [kW] in the HX1 and HX2 heat exchangers respectively over the time period T. Table 3 reports further design specifications of the Bc-prototype components.

In the experimental setup adopted in this study, temperatures, pressure, nitrogen mass flow and electrical power were directly evaluated by specific measurement devices. The enthalpy instead was retrieved by using NIST REFPROP® Version 9.1, referencing the nitrogen gaseous properties [48]. The thermal capacity, COP and TER were derived from dedicated equations. The uncertainty ΔY of the derived parameters was evaluated using Eq. (3) [49]:

$$\Delta Y = \sqrt{\sum_i^N \left(\frac{\delta Y}{\delta X_i}\right)^2 \cdot \Delta X_i^2} \tag{3}$$

where ΔX_i represents the accuracy of the directly measured parameters X, for a total number N of parameters involved in the derived evaluation. The accuracy of the instruments and the uncertainties quantities involved in the experimental tests are collected in Table 4. The maximum uncertainty for the derived parameters is ±2.3 %.

In order to evaluate the specific performance within the thermodynamic cycle, the performance of each component was assessed by using the conservation of energy for one-inlet one-outlet control volume with one-dimensional flow. The steady-state conditions were considered as well as the heat losses across the components, while the potential and kinetic energy terms were neglected. The steady-state form of the energy balance was used to describe the thermodynamic model of each cycle component. In the case of both the compressors and the turbine, the energy balance can be expressed using Eq. (4) as follows

$$\dot{W} = \dot{m}_n \times |h_{out} - h_{in}| \tag{4}$$

where $\dot{W}$ is the net rate of energy transfer by work across the machinery [W], $\dot{m}_n$ is the nitrogen mass flow rate [kg s^{-1}], and $(h_{out} - h_{in})$ accounts for the difference in the nitrogen specific enthalpy [kJ kg^{-1}] between

the outlet and inlet points. The specific enthalpy is a function of both temperature and pressure which, at the machinery outlet, depend on isentropic efficiency η (see Appendix A) and pressure ratio β respectively.

Regarding the heat exchangers, the net heat rate across the heat exchangers [W] can be expressed using Eq. (5) as follows

$$\dot{Q} = \dot{m}_n \times |h_{out} - h_{in}| \quad (5)$$

where, at the outlet of the heat exchangers, the temperature and pressure depend on the effectiveness ε and pressure drop Δp respectively.

The enthalpy and entropy of the nitrogen were evaluated as a function of the monitored temperature and pressure and by using the NIST reference fluid thermodynamic and transport properties database (REFPROP) for the Matlab® software [50].

2.2. Experimental tests

Two experimental tests were carried out to verify the Bc-prototype performance as a function of different operating conditions.

2.2.1. Design operating conditions

The first test aimed at comparing the real performance of the Bc-prototype with the design ones. Therefore, the Bc-prototype was set to operate at steady-state conditions as reported in § 2.1.1 and Table 3.

2.2.2. Sensitivity analysis

A sensitivity analysis was performed to evaluate how and to what extent the maximum pressure and minimum temperature of the Bc-prototype affect its performance. The sensitivity analysis was divided into two tests as follows:

- *Pressure test.* Four pressure levels were tested at the reciprocating compressor outlet, which are 12.8, 13.4, 14.9 and 16.4 bar. To compare the experimental results when operating at different pressure levels, the turbine outlet temperature was kept constant as much as possible at −85 °C by varying the electric heater power. The adopted turbine outlet temperature was higher than the design one (−120 °C) but this was necessary to operate at steady state conditions according to the pressure level and electric heater power. Since the pressure test was not carried out at design conditions, the pressure levels were selected to guarantee the safety of the operating conditions of the turbine (maximum rotating speed) and a stable turbine outlet temperature.
- *Temperature test.* When the pressure test was completed by operating the Bc-prototype in steady-state conditions at a maximum pressure of 16.4 bar and a minimum temperature of −85 °C, the temperature tests began. Specifically, the maximum pressure was kept constant at 16.4 bar and the electric power reduced, thus causing a temperature reduction at the turbine outlet. A minimum temperature lower than −140 °C was reached at the turbine outlet.

The inlet pressure of the reciprocating compressor was about 9 bar during all tests.

3. Results and discussion

This section reports the results of the data monitored during the experimental tests. For each test, the time-temperature and time-pressure plots are reported for the reciprocating compressor and the bootstrap unit (turbine and centrifugal compressor) together with tables where the Bc-prototype performance is summarised.

3.1. Design operating conditions

Figs. 3 and 4 report the pressure and temperature data at the inlet and outlet of the reciprocating compressor (K1), turbine, and centrifugal compressor (K2). The experiment took about 45 min, including the reciprocating compressor start-up and the cycle cooling phases.

At the reciprocating compressor start-up, area -A- in Figs. 3–4, the V1 and V2 valves were opened and closed respectively, thus the nitrogen flowed inside the by-pass circuit. When the reciprocating compressor reached a stable condition in terms of operating pressure at both outlet (about 16.4 bar) and inlet (about 9 bar), which means a pressure ratio of 1.82, the V1 and V2 valves started closing and opening simultaneously (event #1 in Figs. 3–4). At the V2 valve opening, part of the nitrogen flow rate flowed into the turbine (expansion phase, see Fig. 4a and b) and the cycle cooling phase began (area -B- in Figs. 3–4). This latter phase lasted about 15 min in which the cycle control panel

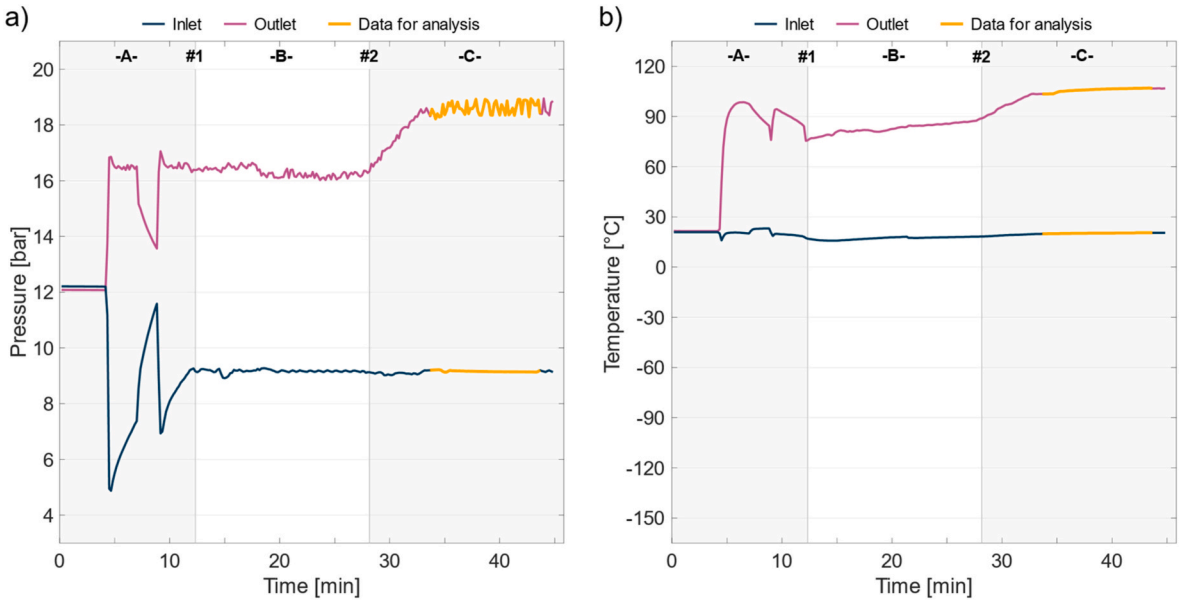

Fig. 3. Data monitored at the inlet and outlet of the reciprocating compressor. Part a) refers to the pressure data while part b) refers to the temperature data. The yellow solid lines represent the data used to evaluate the Bc-prototype performance at design operating conditions. (For interpretation of the references to colour in this figure legend, the reader is referred to the Web version of this article.)

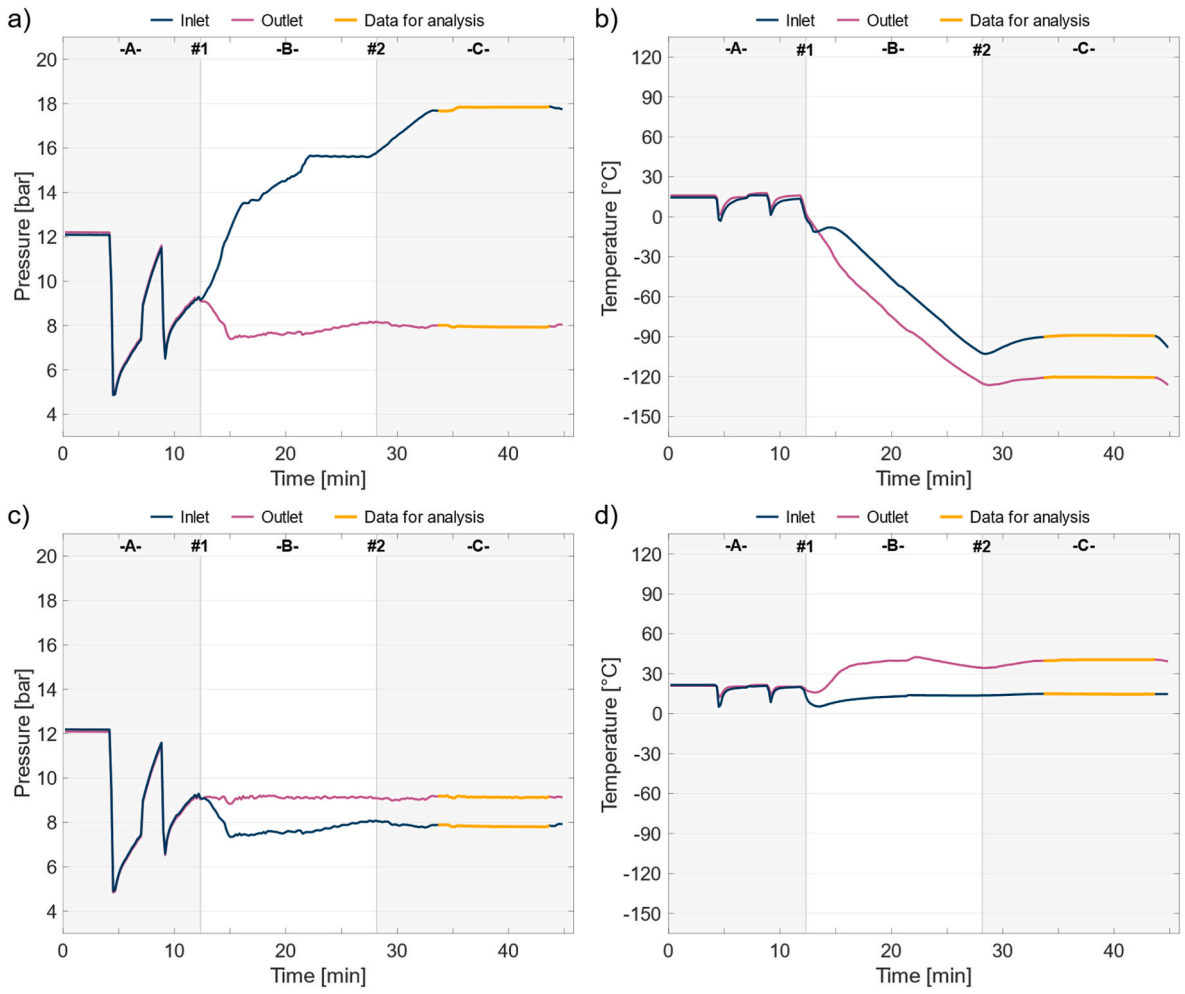

Fig. 4. Data monitored at the inlet and outlet of the turbine and centrifugal compressor. Parts a) and b) refer respectively to the pressure and temperature data of the turbine, while parts c) and d) to the pressure and temperature data of the centrifugal compressor respectively. The yellow solid lines represent the data used to evaluate the Bc-prototype performances at design operating conditions. (For interpretation of the references to colour in this figure legend, the reader is referred to the Web version of this article.)

automatically regulated the V1 and V2 valves according to the speed and outlet temperature of the turbine. The temperature reduction rate at the turbine outlet was on average 8 °C min^{-1}. Fig. 4c and d report the pressure and temperature data of the centrifugal compressor, which provided a pressure ratio of 1.13 thanks to the mechanical work provided by the turbine. When the turbine outlet temperature reached about −120 °C (Fig. 4b), the electric heater was switched on (event #2 in Figs. 3–4) to get a steady-state condition in terms of the cycle minimum temperature. At the electric heater start-up, the V1 and V2 valves were fully closed and opened respectively, and the nitrogen flow rate gradually increased, using the V3 valve to the design value of 0.525 kg s^{-1}. According to the nitrogen flow rate increment, the outlet pressure of the reciprocating compressor increased until reaching the design value of about 18.5 bar with a pressure ratio equal to 2.06.

The data highlighted in yellow in area -C- of Figs. 3–4 refer to the Bc-prototype when considered to be operating at design steady-state conditions in terms of pressure and temperature. Then, the selected data was averaged, and the results reported in Table B1 (see Appendix B) together with the enthalpy [kJ kg^{-1}] and entropy [kJ kg^{-1} K^{-1}] values. The enthalpy and entropy were obtained by using the NIST tables in the Matlab environment. The Bc-prototype performance, evaluated according to Eqs. (2) and (3) and Eqs. (A.1-A.3), are reported in Table 5 and can be summarised as follows:

- The power provided by the electric heater to simulate the cooling effect was 15.6 kW and the power required by the electric motor to run the reciprocating compressor was 53.7 kW. Therefore, the COP of the Bc-prototype was equal to 0.29, which is higher (+16 %) than the design performance reported in § 2.1.1. The electric motor power was about 23 % lower than the design one.
- A thermal power of 45.3 and 11.1 kW was rejected by the nitrogen in the aftercooler (HX1) and intercooler (HX2) respectively at low thermal level. For example, such a thermal power could be recovered for pre-heating water, an operation largely used in the food industry [51]. Considering both the cooling effect and the thermal power, the TER of the Bc-prototype is 1.34.
- The isentropic efficiency of the reciprocating compressor (η_{K1}) was higher than the design one (+10 %). Please notice that the nitrogen temperature measured at the reciprocating compressor outlet is affected by the lubricating oil used to cool the cylinders heads; this involves a difference between the computed isentropic efficiency and the nominal one.
- The isentropic efficiency of the bootstrap unit was lower than expected. In particular, the turbine (η_{T1}) and compressor (η_{K2}) efficiency were 5 % and 9 % lower than the design values respectively. The inlet turbine temperature was indeed lower than the nominal one, thus causing a reduction in the expansion work and therefore different working conditions from the expected ones.

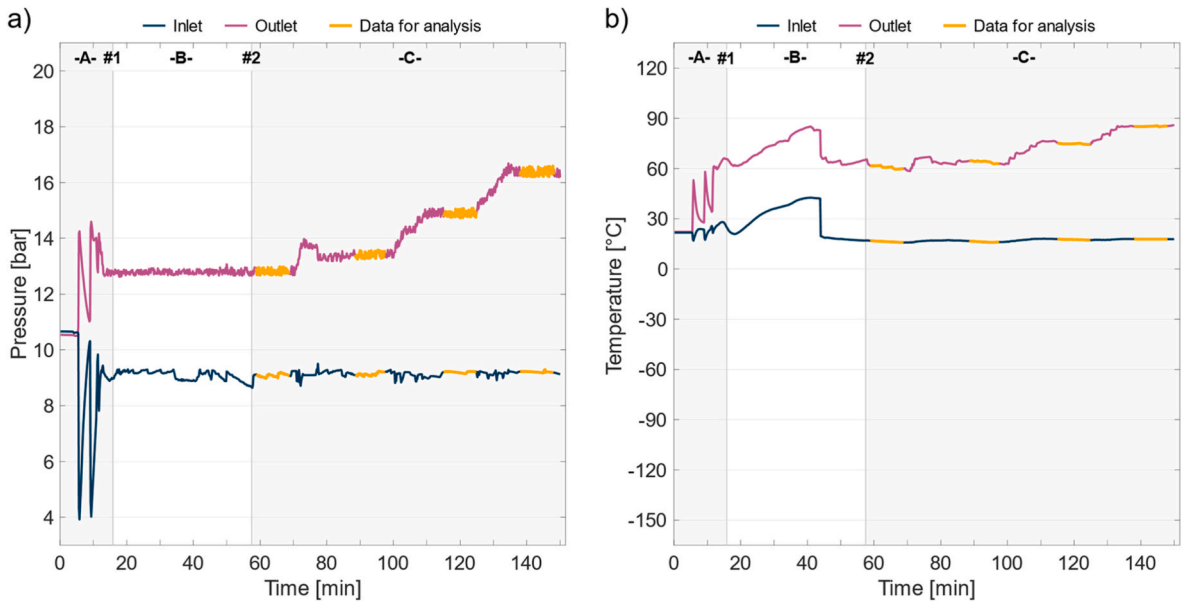

Fig. 5. Data monitored at the inlet and outlet of the reciprocating compressor during the pressure test. Part a) refers to the pressure data while part b) refers to the temperature data. The yellow solid lines represent the data used to evaluate the Bc-prototype performance. (For interpretation of the references to colour in this figure legend, the reader is referred to the Web version of this article.)

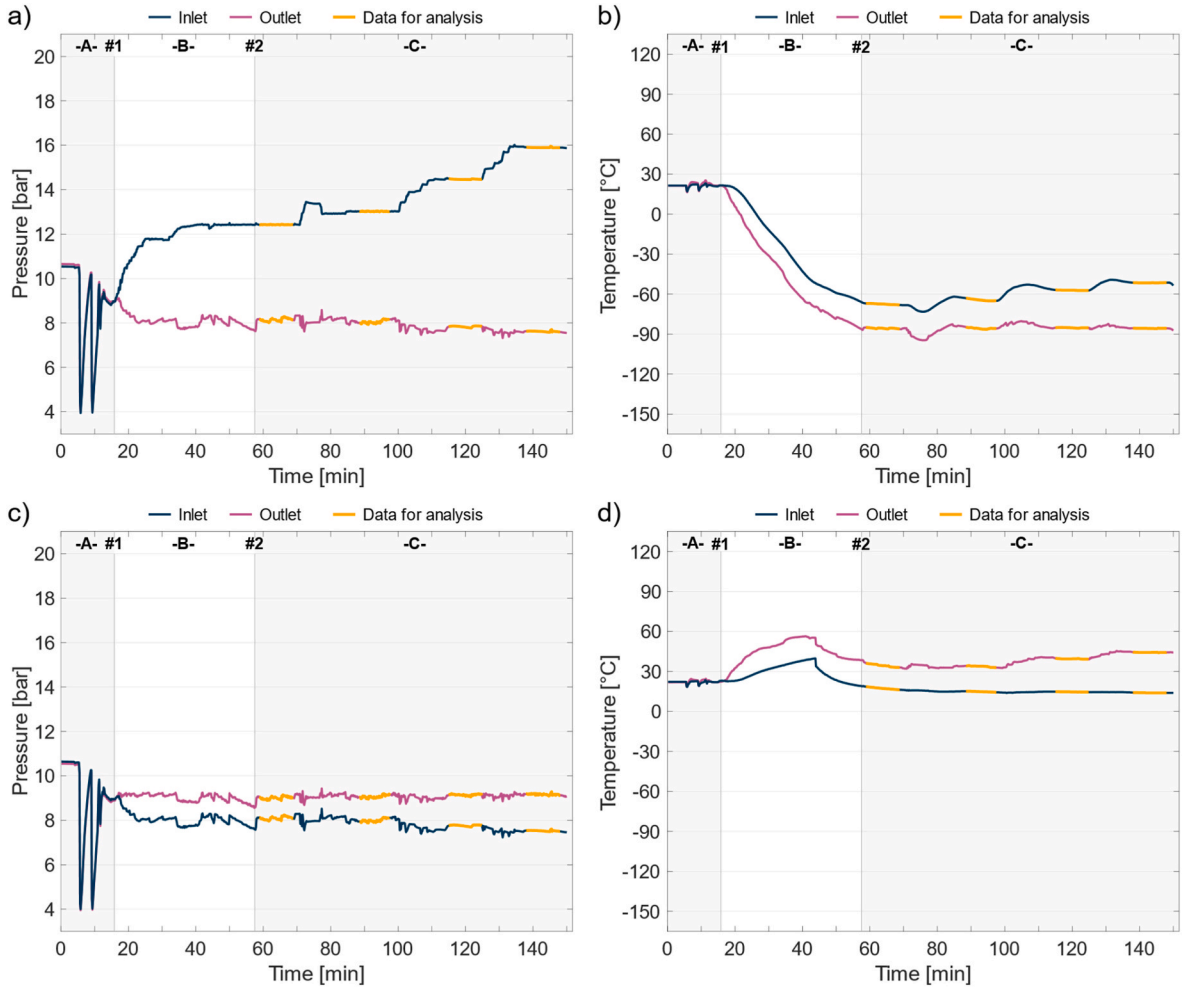

Fig. 6. Data monitored at the inlet and outlet of the turbine and centrifugal compressor during the pressure test. Parts a) and b) refer respectively to the pressure and temperature data of the turbine, while parts c) and d) to the pressure and temperature data of the centrifugal compressor respectively. The yellow solid lines represent data used to evaluate the Bc-prototype performance. (For interpretation of the references to colour in this figure legend, the reader is referred to the Web version of this article.)

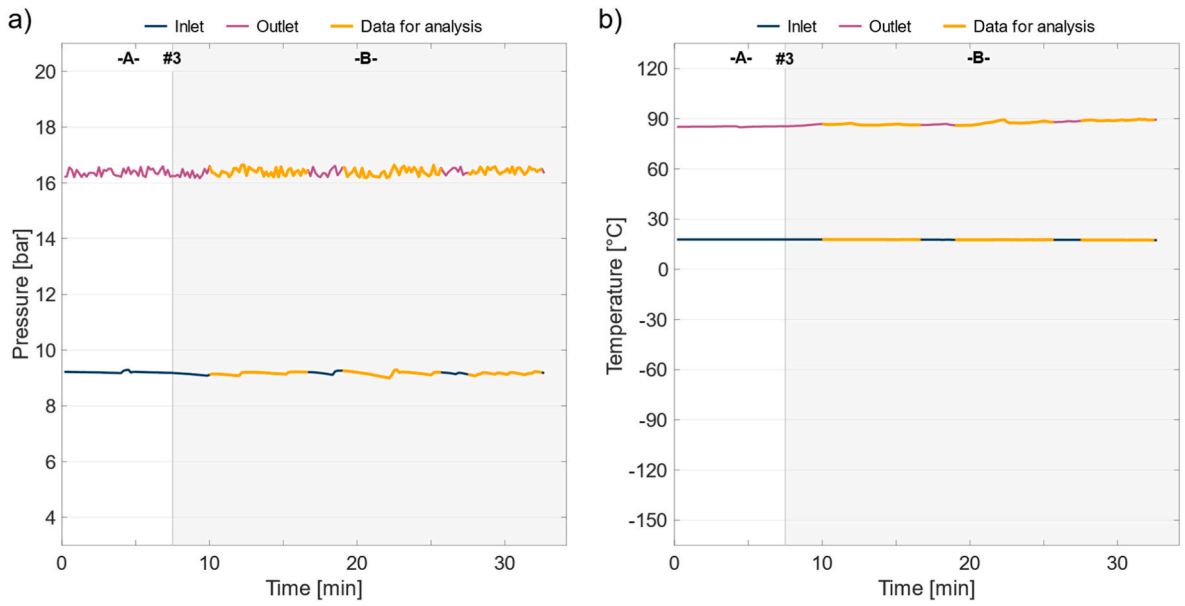

Fig. 7. Data monitored at the inlet and outlet of the reciprocating compressor during the temperature test. Part a) refers to the pressure data while part b) refers to the temperature data. The yellow solid lines represent the data used to evaluate the Bc-prototype performance. (For interpretation of the references to colour in this figure legend, the reader is referred to the Web version of this article.)

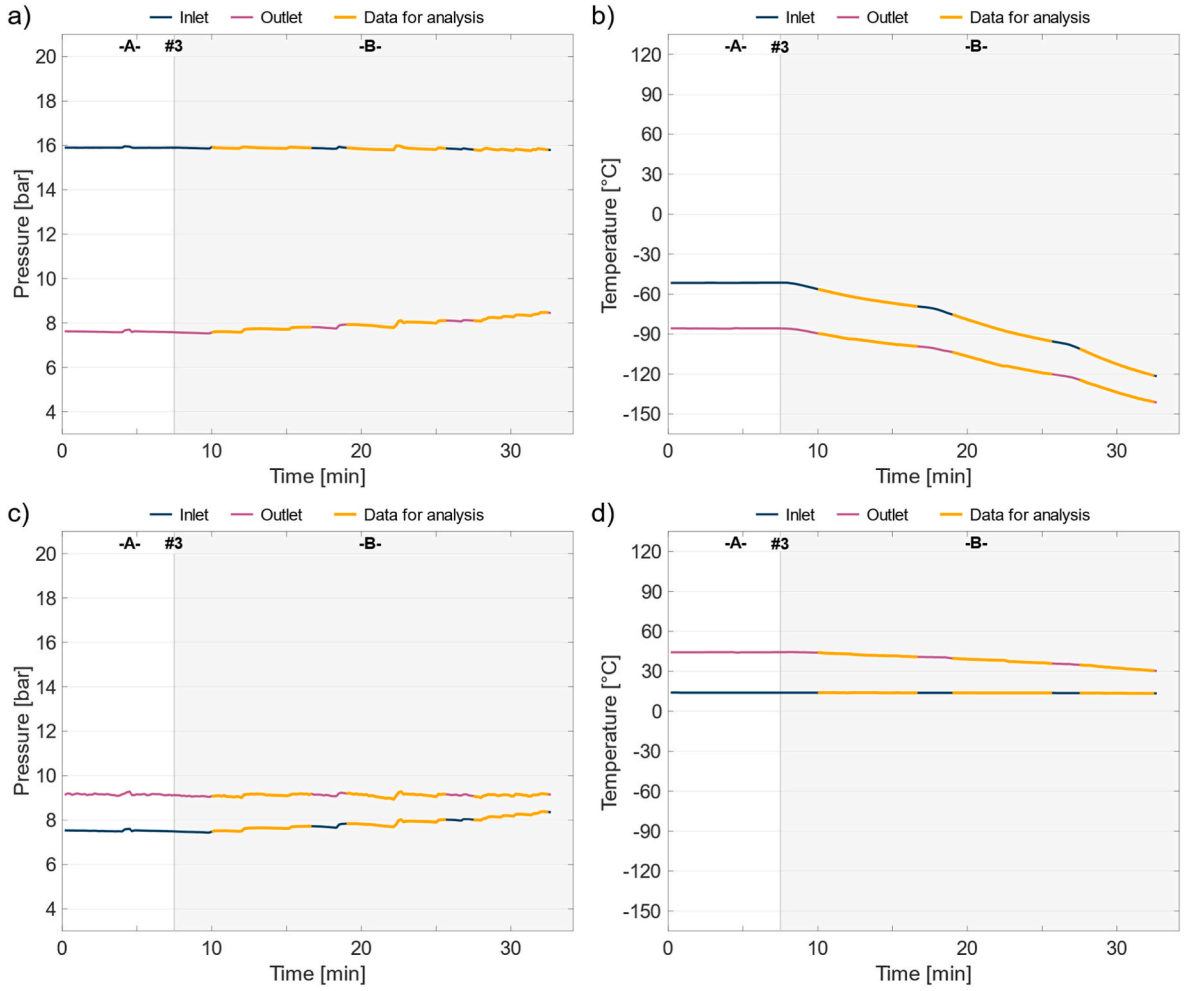

Fig. 8. Data monitored at the inlet and outlet of the turbine and centrifugal compressor during the temperature test. Parts a) and b) refer respectively to the pressure and temperature data of the turbine, while parts c) and d) to the pressure and temperature data of the centrifugal compressor respectively. The yellow solid lines represent the data used to evaluate the Bc-prototype performance. (For interpretation of the references to colour in this figure legend, the reader is referred to the Web version of this article.)

Table 3
Design specifications of the Bc-prototype components.

Component	Data	
Reciprocating compressor (K1)	Suction pressure [bar]	9
	Suction temperature [°C]	20
	Discharge pressure [bar]	18.5
	Discharge temperature [°C]	90
	Isentropic efficiency	0.7
	Power [kW]	65
Turbine (T1)	Suction pressure [bar]	17.5
	Suction temperature [°C]	−80
	Discharge pressure [bar]	7.6
	Discharge temperature [°C]	−120
	Isentropic efficiency	0.8
Centrifugal compressor (K2)	Suction pressure [bar]	7.5
	Suction temperature [°C]	15
	Discharge pressure [bar]	9.25
	Discharge temperature [°C]	45
	Isentropic efficiency	0.6
Aftercooler (HX1)	Type	Shell and tubes
	Exchange surface [m^2]	9
	Maximum pressure [bar]	25
	Design temperature [°C]	−10/+230
	Effectiveness	0.9
	Power [kW]	12
	Pressure drop (nitrogen side) [mbar]	65
	Size [cm]	20 × 35 × 20
Intercooler (HX2)	Type	Shell and tubes
	Exchange surface [m^2]	13
	Maximum pressure [bar]	25
	Design temperature [°C]	−10/+230
	Effectiveness	0.96
	Power [kW]	40
	Pressure drop (nitrogen side) [mbar]	30
	Size [cm]	26 × 35 × 20
Recuperator (HR)	Type	Shell and tubes
	Exchange surface [m^2]	60
	Maximum pressure [bar]	25
	Design temperature [°C]	−200/+100
	Effectiveness	0.95
	Power [kW]	60
	Pressure drop (high pressure side) [mbar]	50
	Pressure drop (low pressure side) [mbar]	150
	Size [cm]	50 × 40 × 70
Electric motor (EM)	Type	Squirrel cage
	Circuit	3 phases
	Power [kW]	70

Table 4
Test devices with accuracy and derived uncertainties of main parameters.

Parameter	Device type	Device model	Accuracy/ Uncertainty
Temperature [K]	T-type thermocouple	IEC 60584–1 compliant	±0.5 K
Pressure [bar]	Pressure transducer	KELLER 23SX	±0.1 % FS
Mass flow, [kg s^{-1}]	Flow sensor	CS INSTRUMENTS VA 550	±1 % of measured value
Power [W]	Power meter	HOBO UX120	±0.5 % FS
Power [W]	Power meter	WattNode 208/240 VAC 3-phase	±0.05 % FS
Enthalpy [kJ kg^{-1}]	[48]	NIST REFPROP Version 9.1	±0.1 %
Thermal capacity [W]	–	Derived	±1.6 %
COP [−]	–	Derived	±2.1 %
TER [−]	–	Derived	±2.3 %

Table 5
Bc-prototype performance when operating at design steady-state conditions. These results were obtained by using the data reported in Table B1.

Components	Pressure and temperature limits $(P_{max}, T_{min}) = (18.6\ bar, -120.5\ ^{\circ}C)$	
	Power [kW]	Efficiency [−]
Reciprocating compressor (K1)	$\dot{W}_{K1} = 46.72$	$\eta_{K1} = 0.772$
Turbine (T1)	$\dot{W}_{T1} = 15.05$	$\eta_{T1} = 0.764$
Centrifugal compressor (K2)	$\dot{W}_{K2} = 14.04$	$\eta_{K2} = 0.548$
Aftercooler (HX1)	$\dot{Q}_{HX1} = 45.32$	$\varepsilon_{HX1} = 0.976$
Intercooler (HX2)	$\dot{Q}_{HX2} = 11.14$	$\varepsilon_{HX2} = 0.793$
Recuperator (RH1)	$\dot{Q}_{RH1} = 61.12$	$\varepsilon_{RH1} = 0.952$
Electric heater (EH)	$\dot{W}_{EH} = 15.19$	–
Electric motor (EM)	$\dot{W}_{EM} = 53.68$	$\zeta = 0.870$ [1]
Nitrogen flow rate [kg s^{-1}]	0.525	
COP	0.290	
TER	1.342	

[1] This includes motor efficiency and mechanical transmission efficiency.

- The heat exchangers, including the recuperator, have high effectiveness in line with the expected one.
- The electric motor efficiency (87 %) includes both the electrical efficiency and the mechanical transmission efficiency.

Under design conditions, operating between a temperature of −120.5 °C at the turbine exhaust and a temperature of 9.5 °C at the heat sink, the Bc-prototype achieved a relative Carnot efficiency of 24.70 %, demonstrating good performance when compared with Brayton cycles [23].

3.2. Sensitivity analysis

A sensitivity analysis was carried out to evaluate how the Bc-prototype performances is affected by the maximum pressure and minimum temperature levels.

3.2.1. Pressure test

The experiment took about 2.5 h including the reciprocating compressor start-up, the Bc-prototype cooling phase, and the tests at four different pressure levels. Figs. 5 and 6 report the monitored data of the pressure and temperature at the inlet and outlet of the reciprocating compressor, turbine, and centrifugal compressor.

Since a problem occurred at the cooling water supply circuit of the aftercooler and intercooler (a valve was not fully opened), the reciprocating compressor start-up and the Bc-prototype cooling phases took about 60 min (area -A- and -B- in Figs. 5 and 6). However, the problem was fixed and the water flow rate in the heat exchangers reactivated; indeed, it can be seen in Figs. 5 and 6b (area -B-) that the temperature profile suddenly drops. The data reported in areas -A- and -B- of Figs. 5 and 6 was obtained by using the same control logic of the Bc-prototype that was explained before in § 3.1.

The pressure test was carried out at four different pressure levels: 12.8, 13.4, 14.9 and 16.4 bar. The yellow lines in area -C- of Figs. 5 and 6 represent the data of the pressure and temperature used to evaluate the Bc-prototype performances. The data refers to about 10 min of monitoring when the Bc-prototype was operating at steady-state conditions, and their average, together with the enthalpy and entropy values, are reported in Tables B.2-B.5. The inlet pressure of the reciprocating compressor (Fig. 5a) and the turbine outlet temperature (Fig. 6b) were kept constant at about 9 bar and −85 °C respectively.

The Bc-prototype performance as a function of four different maximum pressure values is reported in Table 6 and can be summarised as follows:

Table 6
Bc-prototype performance when operating at steady-state conditions during the pressure tests (see yellow solid lines in Figs. 5–6). These results were obtained by using the data reported in Tables B.2-B.5.

Components	Pressure and temperature limits $(\overline{P}_{max}, \overline{T}_{min}) = (12.8\ bar, -85.6\ ^{\circ}C)$		Pressure and temperature limits $(\overline{P}_{max}, \overline{T}_{min}) = (13.4\ bar, -85.7\ ^{\circ}C)$		Pressure and temperature limits $(\overline{P}_{max}, \overline{T}_{min}) = (14.9\ bar, -85.3\ ^{\circ}C)$		Pressure and temperature limits $(\overline{P}_{max}, \overline{T}_{min}) = (16.4\ bar, -85.7\ ^{\circ}C)$	
	Power [kW]	Efficiency [−]	Power [kW]	Efficiency [−]	Power [kW]	Efficiency [−]	Power [kW]	Efficiency [−]
Reciprocating compressor (K1)	$\dot{W}_{K1} = 13.44$	$\eta_{K1} = 0.688$	$\dot{W}_{K1} = 15.43$	$\eta_{K1} = 0.733$	$\dot{W}_{K1} = 21.38$	$\eta_{K1} = 0.759$	$\dot{W}_{K1} = 28.49$	$\eta_{K1} = 0.777$
Turbine (T1)	$\dot{W}_{T1} = 5.10$	$\eta_{T1} = 0.713$	$\dot{W}_{T1} = 6.43$	$\eta_{T1} = 0.782$	$\dot{W}_{T1} = 9.13$	$\eta_{T1} = 0.779$	$\dot{W}_{T1} = 13.54$	$\eta_{T1} = 0.789$
Centrifugal compressor (K2)	$\dot{W}_{K2} = 5.00$	$\eta_{K2} = 0.635$	$\dot{W}_{K2} = 6.13$	$\eta_{K2} = 0.575$	$\dot{W}_{K2} = 8.65$	$\eta_{K2} = 0.586$	$\dot{W}_{K2} = 12.84$	$\eta_{K2} = 0.600$
Aftercooler (HX1)	$\dot{Q}_{HX1} = 13.42$	$\varepsilon_{HX1} = 0.975$	$\dot{Q}_{HX1} = 15.06$	$\varepsilon_{HX1} = 0.979$	$\dot{Q}_{HX1} = 20.93$	$\varepsilon_{HX1} = 0.970$	$\dot{Q}_{HX1} = 28.10$	$\varepsilon_{HX1} = 0.983$
Intercooler (HX2)	$\dot{Q}_{HX2} = 5.37$	$\varepsilon_{HX2} = 0.888$	$\dot{Q}_{HX2} = 5.76$	$\varepsilon_{HX2} = 0.890$	$\dot{Q}_{HX2} = 7.66$	$\varepsilon_{HX2} = 0.861$	$\dot{Q}_{HX2} = 11.34$	$\varepsilon_{HX2} = 0.874$
Recuperator (RH1)	$\dot{Q}_{RH1} = 25.79$	$\varepsilon_{RH1} = 0.949$	$\dot{Q}_{RH1} = 26.51$	$\varepsilon_{RH1} = 0.974$	$\dot{Q}_{RH1} = 28.21$	$\varepsilon_{RH1} = 0.966$	$\dot{Q}_{RH1} = 29.24$	$\varepsilon_{RH1} = 0.968$
Electric heater (EH)	$\dot{W}_{EH} = 6.09$	–	$\dot{W}_{EH} = 6.76$	–	$\dot{W}_{EH} = 9.32$	–	$\dot{W}_{EH} = 13.89$	–
Electric motor (EM)	$\dot{W}_{EM} = 18.75$	$\zeta = 0.717^{(1)}$	$\dot{W}_{EM} = 20.24$	$\zeta = 0.762^{(1)}$	$\dot{W}_{EM} = 25.79$	$\zeta = 0.829^{(1)}$	$\dot{W}_{EM} = 33.8$	$\zeta = 0.843$ [1]
Nitrogen flow rate [kg s^{-1}]	0.291		0.311		0.360		0.407	
COP	0.325		0.334		0.361		0.411	
TER	1.327		1.363		1.470		1.578	

[1] This includes motor efficiency and mechanical transmission efficiency.

Table 7
Bc-prototype performance when operating during the temperature tests (see yellow solid lines in Figs. 7–8). These results were obtained by using the data reported in Tables B.6-B.8.

Components	Pressure and temperature limits $(\overline{P}_{max}, \overline{T}_{min}) = (16.4\ bar, -94.9\ ^{\circ}C)$		Pressure and temperature limits $(\overline{P}_{max}, \overline{T}_{min}) = (16.4\ bar, -112.8\ ^{\circ}C)$		Pressure and temperature limits $(\overline{P}_{max}, \overline{T}_{min}) = (16.4\ bar, -133.4\ ^{\circ}C)$	
	Power [kW]	Efficiency [−]	Power [kW]	Efficiency [−]	Power [kW]	Efficiency [−]
Reciprocating compressor (K1)	$\dot{W}_{K1} = 29.77$	$\eta_{K1} = 0.765$	$\dot{W}_{K1} = 31.86$	$\eta_{K1} = 0.753$	$\dot{W}_{K1} = 35.36$	$\eta_{K1} = 0.741$
Turbine (T1)	$\dot{W}_{T1} = 12.54$	$\eta_{T1} = 0.774$	$\dot{W}_{T1} = 10.69$	$\eta_{T1} = 0.741$	$\dot{W}_{T1} = 8.73$	$\eta_{T1} = 0.709$
Centrifugal compressor (K2)	$\dot{W}_{K2} = 12.33$	$\eta_{K2} = 0.528$	$\dot{W}_{K2} = 10.08$	$\eta_{K2} = 0.519$	$\dot{W}_{K2} = 8.18$	$\eta_{K2} = 0.516$
Aftercooler (HX1)	$\dot{Q}_{HX1} = 29.42$	$\varepsilon_{HX1} = 0.984$	$\dot{Q}_{HX1} = 31.40$	$\varepsilon_{HX1} = 0.974$	$\dot{Q}_{HX1} = 34.77$	$\varepsilon_{HX1} = 0.983$
Intercooler (HX2)	$\dot{Q}_{HX2} = 10.76$	$\varepsilon_{HX2} = 0.866$	$\dot{Q}_{HX2} = 8.40$	$\varepsilon_{HX2} = 0.847$	$\dot{Q}_{HX2} = 6.28$	$\varepsilon_{HX2} = 0.811$
Recuperator (RH1)	$\dot{Q}_{RH1} = 35.46$	$\varepsilon_{RH1} = 0.953$	$\dot{Q}_{RH1} = 48.53$	$\varepsilon_{RH1} = 0.945$	$\dot{Q}_{RH1} = 66.58$	$\varepsilon_{RH1} = 0.921$
Electric heater (EH)	$\dot{W}_{EH} = 12.84$	–	$\dot{W}_{EH} = 10.91$	–	$\dot{W}_{EH} = 8.77$	–
Electric motor (EM)	$\dot{W}_{EM} = 35.20$	$\zeta = 0.846^{(1)}$	$\dot{W}_{EM} = 37.39$	$\zeta = 0.852^{(1)}$	$\dot{W}_{EM} = 41.17$	$\zeta = 0.859$ [1]
Nitrogen flow rate [kg s^{-1}]	0.417		0.439		0.475	
COP	0.365		0.292		0.213	
TER	1.506		1.356		1.210	

[1] This includes motor efficiency and mechanical transmission efficiency.

- The data can be compared as the turbine outlet temperature and reciprocating compressor inlet pressure were kept constant as much as possible at −85 °C and 9 bar respectively.
- The power required by the electric motor to run the reciprocating compressor increased from 18.8 to 33.8 kW (+79.8 %) when increasing the cycle maximum pressure from 12.8 to 16.4 bar (+28.1 %). However, the COP of the Bc-prototype significantly increased from 0.325 to 0.411 (+26.5 %).
- The increment in the COP values, when operating at high pressure, is due to both a higher electric heater power supply, which simulates the cooling effect, and to a higher isentropic efficiency of the reciprocating compressor and turbine (close to the design ones). The isentropic efficiency of the centrifugal compressor was on average equal to 0.6.
- The TER of the Bc-prototype, thus including the heat that could be recovered in the aftercooler (HX1) and intercooler (HX2), increased from 1.327 to 1.578 (+18.9 %).

3.2.2. Temperature test

The temperature test was carried out after the pressure test without turning off the Bc-prototype. In the temperature test, the maximum pressure of the cycle was kept constant at 16.4 bar. The pressure and temperature data in the -A- area of Figs. 7 and 8 refers to the Bc-prototype when operating at a maximum pressure of 16.40 bar and a minimum temperature of −85 °C.

The temperature test took about 30 min and began when the electric heater power was reduced (event #3 in Figs. 7 and 8). Since the maximum pressure was kept constant at 16.4 bar (Fig. 7a), a temperature drop at the turbine outlet occurred after each electric heater power reduction (Fig. 8b). Specifically, the electric heater power was reduced from 13.9 to 8.8 kW (−36.9 %). The data used to evaluate the Bc-prototype performances was highlighted in yellow in area -B- of Figs. 7 and 8, and the average values reported in Tables B.6-B.8.

Table 7 shows the Bc-prototype performance, which can be summarised as follows:

- The electric heater power was first reduced from 13.9 to 12.8 kW (−7.6 %), and then to 10.9 (−21.5 %) and 8.8 (−36.9 %) kW. The average temperature at the turbine outlet thus decreased from −85 to −95 (−11.8 %), −113 (−32.9 %), and −133 (−56.5 %) °C respectively (Fig. 8b). Please notice that the turbine outlet temperature was not constant during the test as the electric heater power was insufficient to get steady-state conditions, therefore the data was averaged. A minimum temperature at the turbine outlet of about −140 °C was reached.
- The temperature reduction rates at the turbine outlet were 1.4, 2.4 and 3.1 °C min^{-1} when operating with an electric power heater of 12.8, 10.9 and 8.8 kW respectively.
- The COP of the Bc-prototype decreased significantly during the temperature test. In particular, the COP was 0.411 (Table 5) when operating at a minimum temperature of −85 °C and then decreased to 0.365 (−11.2 %), 0.292 (−29 %) and 0.213 (−48.2 %) according

to the reduction of the turbine outlet temperature. The TER also decreased from 1.578 (Table 5) to 1.506 (−4.6 %), 1.356 (−14.1 %) and 1.21 (−23.3 %).
- The turbine isentropic efficiency decreased with the reduction of the outlet temperature until a value of about 0.71 (−10.1 %). Furthermore, the isentropic efficiency of centrifugal compressor was very low and almost constant at 0.52.

4. Conclusions

Reducing the temperature at low values is very energy consuming, and nowadays energy consumption is one of the major policy drivers for many governments. This paper reports both the description of a Brayton cryocooler prototype, designed for several industrial applications when temperatures in the range 140–180 K are required, and the data from an experimental campaign where it was tested. To be able to accurately identify and give evidence of the real prototype performance, a first test was conducted at design operating conditions, which are:

- A maximum and minimum pressure of about 18.5 and 8 bar respectively.
- A minimum temperature of −120 °C.
- A cooling effect of about 16 kW.

The pressure range and configuration, with a reciprocating compressor downstream of the bootstrap unit, of the prototype are innovative when compared to standard Brayton cryocoolers operating in the 140–180 K temperature range. The data shows that the coefficient of performance at design conditions is 0.29 without considering about 55 kW of waste heat that can be recovered at low temperatures (<100 °C). Moreover, the adopted working fluid is not air, as adopted in many literature works, but nitrogen, in order to avoid any condensation phenomena. The prototype could be used for several industrial applications such as liquefaction, air conditioning, medical purposes (e.g. covid-19 vaccine storing), and also in the food industry to freeze different food products at very low temperatures as we presented in Ref. [24].

A sensitivity analysis was also carried out to evaluate how and to what extent the prototype performance is affected by the operating conditions. The results demonstrate that:

- The higher the maximum pressure, the higher the prototype performance is. Please consider that the suction nitrogen pressure of the reciprocating compressor was kept constant at about 9 bar. This set up is innovative and prevents the plant from possible ambient air infiltration.
- A temperature of about −140 °C was reached at the turbine outlet. The prototype could have reached a temperature lower than −140 °C but the experiment was stopped to prevent any possible issues with the bootstrap unit (turbine and centrifugal compressor), which is the most expensive component of the prototype (about 70,000 €).
- The centrifugal compressor has a very low isentropic efficiency. However, most of the prototype components were not realised *ad hoc* for the prototype but they were selected on the market.

Based on the presented results, it can be concluded that the prototype has a high energy performance and overcomes the limits presented by other works in the literature (e.g. humidity condensation). The prototype also makes it possible to recover large amounts of waste heat at a low temperature level, which is a huge advantage for applications in the food industry. The prototype performance could be further increased by an *ad hoc* design of both the bootstrap unit and reciprocating compressor. This would make it possible to improve the expansive phase and to better recover the work produced by the turbine. The transmission losses between the reciprocating compressor and the electric motor could be reduced and the oil used to lubricate the reciprocating compressor cooled by using water. Therefore, the coefficient of performance at design conditions could exceed the 0.3 value.

Funding

This research was partially supported by the CRYOFOOD project “Sistemi per la surgelazione rapida degli alimenti basati su cicli ad aria monofasici” (POR FESR 2014–2020, Polo Innovazione AgriFood). Data analysis is part of the project NODES which has received funding from the MUR – M4C2 1.5 of PNRR funded by the European Union - NextGenerationEU (Grant agreement no. ECS00000036).

CRediT authorship contribution statement

Alessandro Biglia: Conceptualization, Data curation, Formal analysis, Investigation, Methodology, Software, Validation, Visualization, Writing - original draft. **Matteo Bilardo:**Investigation, Methodology, Software, Visualization, Writing – original draft, Formal analysis, Data curation. **Lorenzo Comba:** Software, Visualization, Writing – review & editing. **Davide Ricauda Aimonino:** Conceptualization, Investigation, Writing – review & editing. **Marco Grella:** Visualization, Writing – review & editing. **Enrico Fabrizio:** Conceptualization, Funding acquisition, Supervision, Resources, Writing – review & editing. **Paolo Gay:** Conceptualization, Funding acquisition, Project administration, Supervision, Data curation, Resources, Writing – review & editing.

Declaration of competing interest

The authors declare that they have no known competing financial interests or personal relationships that could have appeared to influence the work reported in this paper.

Data availability

The data that has been used is confidential.

Acknowledgements

The authors would like to acknowledge Criotec Impianti S.p.A., Dyria Sistemi S.r.l., La Monfortina S.r.l., and ZOPPI S.r.l. for their valuable collaboration.

Appendix A

The isentropic efficiency of the compressors (η_c) and turbine (η_t) are defined as

$$\eta_c = \frac{h_{out,is}(T_{is}, p) - h_{in}(T, p)}{h_{out}(T, p) - h_{in}(T, p)} \tag{A.1}$$

and

$$\eta_t = \frac{h_{out}(T,p) - h_{in}(T,p)}{h_{out,is}(T_{is},p) - h_{in}(T,p)} \quad (A.2)$$

where $h_{out,is}$ is the outlet enthalpy [kJ kg^{-1}] at isentropic conditions, h_{out} is the outlet enthalpy [kJ kg^{-1}] and h_{in} is the inlet enthalpy [kJ kg^{-1}].

The heat exchangers effectiveness ε is defined as

$$\varepsilon = \frac{h_{out}(T,p) - h_{in}(T,p)}{\Delta h_{max}(T,p)} \quad (A.3)$$

where Δh_{max} is the maximum enthalpy difference [kJ kg^{-1}] obtained if the temperature of the hot fluid exiting the heat exchanger is equal to the temperature of the cold fluid entering the heat exchanger.

Appendix B. This Appendix reports the average values of the data monitored (pressure and temperature) during the tests

Table B.1
Thermodynamic parameters of the Bc-prototype when operating at design steady-state conditions (see Figs. 3–4 and Table 5).

Points [1]	Pressure [bar]	Temperature [°C]	Enthalpy [kJ kg^{-1}]	Entropy [kJ kg^{-1} K^{-1}]
1	9.06	20.26	302.48	6.16
2	18.60	105.91	391.47	6.22
3	18.20	98.10	383.24	6.20
4	18.17	16.98	296.91	5.94
5	17.81	−89.18	180.49	5.44
6	7.95	−120.53	151.83	5.50
7	7.87	−94.53	180.52	5.68
8	7.82	14.73	296.94	6.19
9	9.16	40.40	323.69	6.23

[1] Point numbers are reported in Fig. 2b.

Table B.2
Thermodynamic parameters of the Bc-prototype when operating at a maximum pressure of 12.8 bar during the pressure test (see Figs. 5–6 and Table 6).

Points [1]	Pressure [bar]	Temperature [°C]	Enthalpy [kJ kg^{-1}]	Entropy [kJ kg^{-1} K^{-1}]
1	9.01	16.32	298.33	6.15
2	12.81	60.77	344.52	6.19
3	12.72	58.65	342.29	6.18
4	12.70	16.61	296.18	6.04
5	12.42	−67.52	207.54	5.68
6	8.14	−85.63	190.02	5.72
7	8.11	−70.09	210.96	5.83
8	8.09	15.02	299.60	6.19
9	9.09	33.82	316.77	6.21

[1] Point numbers are reported in Fig. 2b.

Table B.3
Thermodynamic parameters of the Bc-prototype when operating at a maximum pressure of 13.4 bar during the pressure test (see Figs. 5–6 and Table 6).

Points [1]	Pressure [bar]	Temperature [°C]	Enthalpy [kJ kg^{-1}]	Entropy [kJ kg^{-1} K^{-1}]
1	9.06	16.18	298.17	6.15
2	13.42	63.97	347.80	6.19
3	13.31	60.67	344.33	6.18
4	13.30	14.98	295.91	6.03
5	13.02	−64.41	210.66	5.69
6	8.05	−85.72	189.98	5.72
7	8.03	−66.53	211,71	5.83
8	8.00	14.09	296.96	6.18
9	9.13	33.73	316.68	6.21

[1] Point numbers are reported in Fig. 2b.

Table B.4
Thermodynamic parameters of the Bc-prototype when operating at a maximum pressure of 14.9 bar during the pressure test (see Figs. 5–6 and Table 6).

Points [1]	Pressure [bar]	Temperature [°C]	Enthalpy [kJ kg^{-1}]	Entropy [kJ kg^{-1} K^{-1}]
1	9.15	17.54	299.59	6.15
2	14.88	74.77	358.99	6.19
3	14.77	70.48	354.47	6.18
4	14.75	15.70	296.33	6.00
5	14.47	−57.15	217.96	5.69
6	7.84	−85.26	192.59	5.73
7	7.80	−59.72	218.48	5.87

(continued on next page)

Table B.4 (*continued*)

Points [1]	Pressure [bar]	Temperature [°C]	Enthalpy [kJ kg^{-1}]	Entropy [kJ kg^{-1} K^{-1}]
8	7.77	14.63	296.85	6.19
9	9.20	37.74	320.88	6.22

[1] Point numbers are reported in Fig. 2b.

Table B.5
Thermodynamic parameters of the Bc-prototype when operating at a maximum pressure of 16.4 bar during the pressure test (see Figs. 5–6 and Table 6).

Points	Pressure [bar]	Temperature [°C]	Enthalpy [kJ kg^{-1}]	Entropy [kJ kg^{-1} K^{-1}]
1	9.16	17.80	299.86	6.15
2	16.37	85.25	369.87	6.19
3	16.22	80.07	364.40	6.18
4	16.20	15.10	295.35	5.97
5	15.90	−51.54	223.50	5.69
6	7.62	−85.72	190.22	5.74
7	7.59	−53.91	224.34	5.91
8	7.53	13.95	296.19	6.20
9	9.21	44.24	327.73	6.24

Table B.6
Thermodynamic parameters of the Bc-prototype when operating at an average minimum temperature of −94.9 °C during the temperature test (see Figs. 7–8 and Table 7).

Points [1]	Pressure [bar]	Temperature [°C]	Enthalpy [kJ kg^{-1}]	Entropy [kJ kg^{-1} K^{-1}]
1	9.12	17.78	299.85	6.15
2	16.40	86.55	371.24	6.20
3	16.21	81.50	365.92	6.19
4	16.20	15.11	295.36	5.97
5	15.89	−63.53	210.32	5.63
6	7.71	−94.88	180.24	5.68
7	7.67	−67.44	211.03	5.84
8	7.61	13.86	296.07	6.19
9	9.17	42.25	325.65	6.24

[1] Point numbers are reported in Fig. 2b.

Table B.7
Thermodynamic parameters of the Bc-prototype when operating at an average minimum temperature of −112.8 °C during the temperature test (see Figs. 7–8 and Table 7).

Points [1]	Pressure [bar]	Temperature [°C]	Enthalpy [kJ kg^{-1}]	Entropy [kJ kg^{-1} K^{-1}]
1	9.11	17.64	299.70	6.15
2	16.38	87.52	372.27	6.20
3	16.19	82.41	366.89	6.198
4	16.17	15.11	295.37	5.97
5	15.85	−86.38	184.83	5.50
6	7.96	−112.75	160.48	5.55
7	7.92	−91.19	185.33	5.68
8	7.87	13.73	295.87	6.18
9	9.19	35.80	318.84	6.21

[1] Point numbers are reported in Fig. 2b.

Table B.8
Thermodynamic parameters of the Bc-prototype when operating at an average minimum temperature of −133.4 °C during the temperature test (see Figs. 7–8 and Table 7).

Points [1]	Pressure [bar]	Temperature [°C]	Enthalpy [kJ kg^{-1}]	Entropy [kJ kg^{-1} K^{-1}]
1	9.10	17.49	299.55	6.15
2	16.44	89.15	373.99	6.20
3	16.18	84.08	368.66	6.19
4	16.16	15.20	295.47	5.97
5	15.81	−111.97	155.30	5.33
6	8.30	−133.41	136.92	5.39
7	8.26	−119.97	155.38	5.47
8	8.20	13.50	295.55	6.17
9	9.18	30.04	312.77	6.19

[1] Point numbers are reported in Fig. 2b.

References

[1] Walker G. Joule-Thomson cooling systems. Cryocoolers. In: The International cryogenics monograph series. Boston, MA: Springer; 1983. p. 265–95. https://doi.org/10.1007/978-1-4899-5286-8_6.

[2] Walker G. Claude and Joule-Brayton systems. Cryocoolers. The International cryogenics monograph series, vols. 297–353. Boston, MA: Springer; 1983. https://doi.org/10.1007/978-1-4899-5286-8_6.

[3] Walker G, Senft JR. Free-piston stirling engines. Lecture Notes in engineering, vol. 12. Berlin, Heidelberg: Springer; 1985. p. 23–99. https://doi.org/10.1007/978-3-642-82526-2_2.

[4] Gifford WE. The Gifford-McMahon cycle. Advances in cryogenic engineering, vol. 11. Boston, MA: Springer; 1966. p. 152–9. https://doi.org/10.1007/978-1-4757-0522-5_16.

[5] Mikulin EI, Tarasov AA, Shkrebyonock MP. Low-temperature expansion pulse tubes. Advances in cryogenic engineering, vol. 29. Boston, MA: Springer; 1984. p. 629–37. https://doi.org/10.1007/978-1-4613-9865-3_72.

[6] Choi YS, Kim DL, Shin DW. Cool-down characteristic of conduction-cooled superconducting magnet by a cryocooler. Physica C: Superconductivity and its Applications 2011;471:1440–4. https://doi.org/10.1016/j.physc.2011.05.212.

[7] Qiao X, Sun D, Zhang J, Qi Y, Su S, Wang C, et al. Numerical study on a two-stage large cooling capacity stirling cryocooler working at 20 K. Cryogenics 2021;118:103334. https://doi.org/10.1016/j.cryogenics.2021.103334.

[8] Hirabayashi M, Narasaki K, Tsunematsu S, Kimura Y, Yoshida S, Murakami H, et al. Thermal design and its on-orbit performance of the AKARI cryostat. Cryogenics 2008;48:189–97. https://doi.org/10.1016/j.cryogenics.2008.03.003.

[9] Deserranno D, Zagarola M, Li X, Mustafi S. Optimization of a Brayton cryocooler for ZBO liquid hydrogen storage in space. Cryogenics 2014;64:172–81. https://doi.org/10.1016/j.cryogenics.2014.04.025.

[10] Aasadnia M, Mehrpooya M. Large-scale liquid hydrogen production methods and approaches: a review. Appl Energy 2018;212:57–83. https://doi.org/10.1016/j.apenergy.2017.12.033.

[11] Zhang T, Dang H. Investigations on a 1 K hybrid cryocooler composed of a four-stage Stirling-type pulse tube cryocooler and a Joule-Thomson cooler. Part A: Theoretical analyses and modelling. Cryogenics 2021;116:103282. https://doi.org/10.1016/j.cryogenics.2021.103282.

[12] Liu Z, Ma Y, Quan J, Liu Y, Wang J, Li J, et al. Development of a compact 2.17 K hybrid ^{4}He JT cryocooler for space applications. Cryogenics 2021;118:103347. https://doi.org/10.1016/j.cryogenics.2021.103347.

[13] Hu JY, Chen S, Zhu J, Zhang LM, Luo EC, Dai W, et al. An efficient pulse tube cryocooler for boil-off gas reliquefaction in liquid natural gas tanks. Appl Energy 2016;164:1012–8. https://doi.org/10.1016/j.apenergy.2015.03.096.

[14] Jakob G, Lizon JL. Advanced high-cooling power 2-stage Gifford-McMahon refrigerator systems. San Diego, USA: SPIE 7739-158 Astronomical Telescopes and Instrumentation; 2010.

[15] Guo Y, Zhou Q, Liu X, Ding T, Zhang H, Fu Z, et al. Co-designing cryogenic system with pulse tube cryocooler and loop heat pipe for infrared energy management. Appl Therm Eng 2021;195:117228. https://doi.org/10.1016/j.applthermaleng.2021.117228.

[16] Derking JH, Holland HJ, Lerou PPPM, Tirolien T, ter Brake HJM. Micromachined Joule-Thomson cold stages operating in the temperature range 80–250 K. Int J Refrig 2012;35:1200–7. https://doi.org/10.1016/j.ijrefrig.2012.01.008.

[17] Zhu S, Yu G, Li X, Dai W, Luo E. Parametric study of a free-piston Stirling cryocooler capable of providing 350 W cooling power at 80 K. Appl Therm Eng 2020;174:115101. https://doi.org/10.1016/j.applthermaleng.2020.115101.

[18] Xu D, Gong L, Li L, Xu X, Liu H, Huang R. Experimental investigation and optimization of small-scale helium liquefaction with multi-cryocoolers. Cryogenics 2015;69:10–7. https://doi.org/10.1016/j.cryogenics.2015.03.001.

[19] Dorosz P, Chorowski M, Piotrowska A. Performance of the one-stage Joule–Thomson cryocooler fed with a nitrogen–hydrocarbon mixture and built from mass-produced components made for the refrigeration industry. Int J Refrig 2017;82:252–61. https://doi.org/10.1016/j.ijrefrig.2017.06.011.

[20] Deng W, Liu S, Chen X, Ding L, Jiang Z. A work-recovery pulse tube refrigerator for natural gas liquefaction. Cryogenics 2020;111:103170. https://doi.org/10.1016/j.cryogenics.2020.103170.

[21] Spence SWT, Doran WJ, Artt DW. Design, construction and testing of an air-cycle refrigeration system for road transport. Int J Refrig 2004;27:503–10. https://doi.org/10.1016/j.ijrefrig.2004.02.003.

[22] Spence SWT, Doran WJ, Artt DW, McCullough G. Performance analysis of a feasible air-cycle refrigeration system for road transport. Int J Refrig 2005;28:381–8. https://doi.org/10.1016/j.ijrefrig.2004.08.005.

[23] Foster AM, Brown T, Gigiel AJ, Alford A, Evans JA. Air cycle combined heating and cooling for the food industry. Int J Refrig 2011;34:1296–304. https://doi.org/10.1016/j.ijrefrig.2011.03.016.

[24] Biglia A, Messina C, Comba L, Ricauda Aimonino D, Gay P, Brugiapaglia A. Quick-freezing based on a nitrogen reversed Brayton cryocooler prototype: effects on the physicochemical characteristics of beef *longissimus thoracis* muscle. Innov Food Sci Emerg Technol 2022;82:103208. https://doi.org/10.1016/j.ifset.2022.103208.

[25] Dhillon AK, Ghosh P. Performance characteristics map using exergy analysis of reverse Brayton cryocooler for HTS applications: Selection, Optimization, Design and Operational guidelines. Cryogenics 2020;106:103024. https://doi.org/10.1016/j.cryogenics.2019.103024.

[26] Lou J, Wang J, Xia J, Du Y, Zhao P, Zhang G. Thermodynamic analysis of open-air Brayton cycle to predict radial turbine aerodynamic performance. Appl Therm Eng 2023;219:119411. https://doi.org/10.1016/j.applthermaleng.2022.119411.

[27] Chang H-M, Cha Y. Modified Brayton refrigeration cycles for forced-flow cooling of HTS fusion system. 2023 Cryogenics 2023;132:103681. https://doi.org/10.1016/j.cryogenics.2023.103681.

[28] Maytal BZ. On the cryocooling by ideal gases: a review (by the unified model of cryocoolers). Int J Heat Mass Tran 2020;148:118989. https://doi.org/10.1016/j.ijheatmasstransfer.2019.118989.

[29] Bian J, Yang J, Li Y, Chen Z, Liang F, Cao X. Thermodynamic and economic analysis of a novel hydrogen liquefaction process with LNG precooling and dual-pressure Brayton cycle. Energy Convers Manag 2021;250:114904. https://doi.org/10.1016/j.enconman.2021.114904.

[30] Behera BC, Chetan, Ghosh S, Rao PV. The underlying mechanisms of coolant contribution in the machining process. Machining and Tribology 2022:37–66. https://doi.org/10.1016/B978-0-12-819889-6.00003-4.

[31] Conklin JC, Courville GE, Scott JH. Evaluation of active working fluids for Brayton cycles in space applications. AIP Conf Proc 2004;699:463–72. https://doi.org/10.1063/1.1649607.

[32] Yuan Z, Zheng Q, Jiang Y, Jiang B, Luo M. Review on power conversion unit of noble gas closed Brayton cycle for space and underwater applications. Appl Therm Eng 2023;223:119981. https://doi.org/10.1016/j.applthermaleng.2023.119981.

[33] Hou Y, Zhao HL, Chen CZ, Xiong LY. Developments in reverse Brayton cycle cryocooler in China (2006 Cryogenics 2006;46:403–7. https://doi.org/10.1016/j.cryogenics.2005.11.021.

[34] Chang H-M, Chung MJ, Kim MJ, Park SB. Thermodynamic design of methane liquefaction system based on reversed-Brayton cycle. Cryogenics 2009;49:226–34. https://doi.org/10.1016/j.cryogenics.2008.08.006.

[35] Liu Z, Rieder HE, Schmidt C, Mayer M, Guo Y, Winiwarter W, et al. Optimal reactive nitrogen control pathways identified for cost-effective $PM_{2.5}$ mitigation in Europe. Nat Commun 2023;14:4246. https://doi.org/10.1038/s41467-023-39900-9.

[36] Jouhara H, Chauhan A, Guichet V, Delpech B, Abdelkareem MA, Olabi AG, et al. Low-temperature heat transfer mediums for cryogenic applications. J Taiwan Inst Chem Eng 2023;148:104709. https://doi.org/10.1016/j.jtice.2023.104709.

[37] Yildiz Y, Nalbant M. A review of cryogenic cooling in machining processes. Int J Mach Tool Manufact 2008;48:947–64. https://doi.org/10.1016/j.ijmachtools.2008.01.008.

[38] Damir A, Sadek A, Attia H. Characterization of machinability and environmental impact of cryogenic turning of Ti-6Al-4V. Procedia CIRP 2018;69:893–8. https://doi.org/10.1016/j.procir.2017.11.070.

[39] Olumayegun O, Wang M, Kelsall G. Thermodynamic analysis and preliminary design of closed Brayton cycle using nitrogen as working fluid and coupled to small modular Sodium-cooled fast reactor (SM-SFR). Appl Energy 2017;191:436–53. https://doi.org/10.1016/j.apenergy.2017.01.099.

[40] Cao X, Yang J, Zhang Y, Gao S, Bian J. Process optimization, exergy and economic analysis of boil-off gas re-liquefaction processes for LNG carriers. Energy 2022;242:122947. https://doi.org/10.1016/j.energy.2021.122947.

[41] Chen K, Yu H, Fan G, Zhang Y, Dai Y. Multi-objective optimization of a novel combined parallel power generation system using CO_2 and N_2 for cascade recovery of LNG cryogenic energy. Energy Convers Manag 2022;256:115395. https://doi.org/10.1016/j.enconman.2022.115395.

[42] Choi JH, Yoon J, Eoh J, Kim MH, Jo HJ. Performance and size comparison of two-stage and three-stage axial turbines for a nitrogen gas Brayton cycle coupled with a sodium-cooled fast reactor. Nucl Eng Des 2021;380:111309. https://doi.org/10.1016/j.nucengdes.2021.111309.

[43] Biglia A, Comba L, Fabrizio E, Gay P, Ricauda Aimonino D. Case studies in food freezing at very low temperature. Energy Proc 2016;101:305–12. https://doi.org/10.1016/j.egypro.2016.11.039.

[44] Biglia A, Gemmell AJ, Foster HJ, Evans JA. Temperature and energy performance of domestic cold appliances in households in England. Int J Refrig 2018;87:172–84. https://doi.org/10.1016/j.ijrefrig.2017.10.022.

[45] Biglia A, Gemmell AJ, Foster HJ, Evans JA. Energy performance of domestic cold appliances in laboratory and home environments. Energy 2020;204:117932. https://doi.org/10.1016/j.energy.2020.117932.

[46] Biglia A, Comba L, Fabrizio E, Gay P, Mannini A, Mussinatto A, Ricauda Aimonino D. Reversed Brayton cycle for food freezing at very low temperatures: energy performance and optimisation. Int J Refrig 2017;81:82–95. https://doi.org/10.1016/j.ijrefrig.2017.05.022.

[47] Wang C, Sun D, Shen Q, Shen K, Linghu J, Wang X. Techno-economic analysis on nitrogen reverse Brayton cycles for efficient coalbed methane liquefaction process. Energy 2023;280:128167. https://doi.org/10.1016/j.energy.2023.128167.

[48] Span R, Lemmon E, Jacobsen RT, Wagner W, Yokozeki A. A Reference equation of state for the thermodynamic properties of nitrogen for temperatures from 63.151 to 1000 K and pressures to 2200 MPa. J Phys Chem Ref Data 2000;29:1361–433. https://doi.org/10.1063/1.1349047.

[49] Moffat RJ. Describing the uncertainties in experimental results. Exp Therm Fluid Sci 1988;1:3–17. https://doi.org/10.1016/0894-1777(88)90043-X.

[50] National Institute of Standards and Technology (Standard Reference Data). NIST reference fluid thermodynamic and transport properties database: version 10. Gaithersburg, MD: United States Department of Commerce; 2013.

[51] Biglia A, Fabrizio E, Ferrara M, Gay P, Ricauda Aimonino D. Performance assessment of a multi-energy system for a food industry. Energy Proc 2015;82:540–5. https://doi.org/10.1016/j.egypro.2015.11.867.